Ambient Noise Interferometry on Two-Dimensional DAS Arrays

Eileen Martin and Biondo Biondi

ABSTRACT

When using three-component geophones for ambient noise tomography, the process of extracting Rayleigh or Love waves requires first rotating data into radial and transverse components, respectively, before cross-correlation. When a two-dimensional distributed acoustic sensing (DAS) array is used, a single straight line can easily have Rayleigh waves extracted via cross-correlation within the line. However, only using straight lines significanly reduces our ray coverage, so we aim to garner meaninful information from all pairs of channels in the array. In practice, cross-correlation and cross-coherence of the data recorded at many pairs of channels in the Stanford DAS Array-1 (SDASA-1) yield coherence waveforms. But, we can not rotate every data point into radial and transverse components, so special treatment must be given to understand the coherent waveforms generated when non-colinear fibers' data are cross-correlated. This is the first extension of ambient noise theory given these geometric constraints.

INTRODUCTION

When ambient noise interferometry was first catching on, scientist cross-correlated single-component data (Shapiro et al., 2005), then researchers realized they could take any pair of three-component geophones, rotate their data to a radial component in-line with both receivers, then cross-correlate to get Rayleigh surface waves. Less than a decade after the use of amibent noise interferometry began, the theory was extended and shown to work in practice for extraction of Love waves at regional (Lin et al., 2008) and later reservoir (de Ridder, 2014), (Nakata et al., 2015) and engineering (Nakata et al., 2011) scales. The process is similar to Rayleigh wave extraction, although transverse components are cross-correlated.

Over the past few years, fiber optic Distributed Acoustic Sensing (DAS) arrays have begun to emerge as a potentially cost-effective option for permanent or long-term ambient noise collection (Ajo-Franklin et al., 2015), (Martin et al., 2015), (Martin et al., 2016), (Martin et al., 2017c), (Martin et al., 2017b), (Zeng et al., 2017), (Martin et al., 2017a). Although straight fiber optics keep the cost of DAS arrays lower, broadside insensitivity and lowered angular sensitivity relative to geophones is a major limiting factor in their utility (Kuvshinov, 2016). For extracting Rayleigh waves, the theory is

not very different, so we can correlate channels along the same straight line (Martin et al., 2015), (Martin et al., 2016), (Martin et al., 2017c), (Martin et al., 2017b), (Zeng et al., 2017). All of the Rayleigh waves extracted from DAS arrays have been extracted from two-dimensional arrays, so we aim to use the vastly more numerous ray paths between different lines of these arrays so that velocities may be estimated throughout the extent of these arrays. This is the first extension of interferometry of a DAS array to non-colinear channels.

This report develops the theory of ambient noise cross-correlations between straight-fiber DAS channels at arbitrary distances and orientations from each other in section 2. The data extracted are predicted to be a mix of Love and Rayleigh waves in many cases. In section 3 we show results of cross-correlations and cross-coherences throughout the Stanford DAS Array-1 (SDASA-1) (Martin et al., 2017a). Then we conclude, and discuss future extensions of this work.

THEORY

We assume the signal recorded by a DAS channel is the average extensional strain rate along a gauge long subset of fiber, which is equivalent to the difference in the velocities in the direction of the fiber at the end points of that gauge length. We aim to describe the cross-correlation of two DAS signals in terms of cross-correlations of four three-component geophones, one sitting at each end of each of the two channels. Ideally we would follow the procedure used in Lin et al. (2008) to extract radial and transverse components that correspond to Rayleigh and Love waves, respectively, but with the geometric constraints of DAS, we must limit ourselves to only having measurements in one direction.

We start with $C_{geo:s,r}(\tau)$, the cross-correlation of the θ_s component of an $x-y$ oriented 3C geophone at (x_s, y_s) with the θ_r component of another $x-y$ oriented 3C geophone at (x_r, y_r), as pictured in Figure 1a. Let $\mathbf{v}^{(\cdot)}(t)$ be the velocity vector at $(x_\cdot, y_\cdot)$ time t, and let $C_{xy:s,r}(\tau)$ be the cross-correlation of $v_x^s(t)$ with $v_y^r(t)$ (and likewise for other components). We drop the τ to shorten notation from here on. Let $c_\cdot = \cos(\theta_\cdot)$ and $s_\cdot = \sin(\theta_\cdot)$. Then our improperly rotated cross-correlation is:

$$\begin{aligned} C_{geo:s,r} &= \int (v_x^s(t)c_s - v_y^s(t)s_s)(v_x^r(t+\tau)c_r - v_y^r(t+\tau)s_r)dt \\ &= c_s c_r C_{xx:s,r} - c_s s_r C_{xy:sr} - s_s c_r C_{yx:s,r} + s_s s_r C_{yy:s,r} \end{aligned}$$

We can then use a 4x4 matrix as in Lin et al. (2008) to express these cross-correlations in terms of radial and transverse cross-correlations which can be more easily interpreted as Rayleigh and Love waves. This is achieved by rotating by the angle θ_T from the $x-y$ coordinate system into the $T-R$ transverse and radial coordinate system:

$$\begin{aligned} C_{geo:s,r} = C_{tt:s,r}(c_s c_T + s_s s_T)(c_r c_T + s_r s_T) + C_{tr:s,r}(c_s c_T + s_s s_T)(c_r s_T - s_r c_T) \\ + C_{rt:s,r}(c_s s_T - s_s c_T)(c_r c_T + s_r s_T) + C_{rr:s,r}(c_s s_T - s_s c_T)(c_r s_T - s_r c_T). \end{aligned}$$

Consider the case $\theta_r = \theta_s = 0$, which would be relevant to DAS channels on parallel lines, a common configuration (Martin et al., 2016), (Martin et al., 2017c), (Zeng et al., 2017). Note that $\theta_T = 0$ corresponds to two parallel channels directly across from each other ($\theta_{sr} = \pi/2$ in Figure 1b), and $\theta_T = \pi/2$ corresponds to two colinear channels ($\theta_{sr} = 0$ in Figure 1b). In this case, $C_{geos:s,r}$ simplifies to:

$$C_{geos:s,r} = C_{tt:s,r}c_T^2 + c_T s_T(C_{tr:s,r} + C_{rt:s,r}) + C_{rr:s,r}s_T^2$$

In fact, if $\theta_T = 0$, $C_{geos:s,r}$ simplifies to $C_{tt:s,r}$ which extracts a Love wave, and if $\theta_T = \pi/2$, $C_{geos:s,r} = C_{rr:s,r}$ which is a Rayleigh wave (Lin et al., 2008). For all θ_T in between, we extract a mix of Love waves, Rayleigh waves and $(C_{tr:s,r} + C_{rt:s,r})$, quantities which have not been explained in the literature. The visuals in Lin et al. (2008) suggest these may simply increase the noise level, but further investigation is needed to understand the role of these terms.

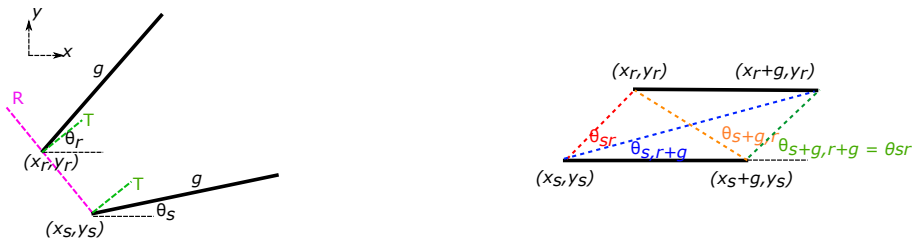

(a) (b)

Figure 1: (Top) The geometry of two DAS channels (thick black lines) is drawn. Both channels use gauge length g, and if there were 3C geophones at their end points, radial R and transverse T components of the data could be used for easy Love and Rayleigh wave extraction. (Bottom) Multiple existing surface DAS arrays have some parallel lines of fibers in them. The angles between the end point pairs of two parallel DAS channels and the x-axis are labeled. [**NR**]

Another common case relevant to perpendicular fibers is $\theta_s = 0$, $\theta_r = \pi/2$. In this case, $C_{geos:s,r}$ simplifies to:

$$C_{geos:s,r} = C_{tt:s,r}c_T s_T - C_{tr:s,r}c_T^2 + C_{rt:s,r}s_T^2 - C_{rr:s,r}s_T c_T$$

If $\theta_T = 0$ or $\pi/2$, i.e. we are at an orthogonal corner or crossing-point in the array, $C_{geos:s,r}$ simplifies to $-C_{tr:s,r}$ or $C_{rt:s,r}$ respetively. In future work, these corner and crossing points may be useful to recognizing these cross terms and understanding their influence throughout the rest of the array. At other angles, we would expect a linear combination of Rayleigh waves, Love waves, and the C_{rt} and C_{tr} cross-terms which are not well understood.

Now we can build from the expression for pairs of improperly rotated 3C geophones

into the actual cross-correlation of two DAS channels. Consider two DAS channels of gauge length g, as in Figure 1a, one extending from (x_s, y_s) to $(x_s + g\cos(\theta_s), y_s + g\sin(\theta_s))$, and the other from (x_r, y_r) to $(x_r + g\cos(\theta_r), y_r + g\sin(\theta_r))$. Using the notation that $s+g$ and $r+g$ are referring to positions $(x_s + g\cos(\theta_s), y_s + g\sin(\theta_s))$ and $(x_r + g\cos(\theta_r), y_r + g\sin(\theta_r))$, their cross-correlation, $C_{DAS:s,r}$ is:

$$C_{DAS:s,r} = C_{geo:s,r} - C_{geo:s+g,r} - C_{geo:s,r+g} + C_{geo:s+g,r+g}$$

Again consider the case of two parallel fibers, $\theta_r = \theta_s = 0$, as pictured in Figure 1b, where channel $\cdot$ runs from $(x_\cdot, y_\cdot)$ to $(x_\cdot + g, y_\cdot)$. Let θ_{sr} be the angle between $(x_r, y_r) - (x_s, y_s)$ and $(x_s + g, y_s) - (x_s, y_s)$, and likewise for $s+g$ and $r+g$. There are two cases where $C_{DAS:s,r}$ simplifies. The first is for two colinear channels, $\theta_{sr} = 0$ (like the Rayleigh wave extraction that has been done in the past):

$$C_{DAS:s,r} = C_{rr:s,r} - C_{rr:s+g,r} - C_{rr:s,r+g} + C_{rr:s+g,r+g},$$

which leads to a Rayleigh wave which has a wavelet that is a bit more ringy than the typical $C_{rr:s,r}$. The other special case is for two parallel channels that line up, $\theta_{sr} = \theta_{s+g,r+g} = \pi/2$. As short notation, let X refer to $\theta_{s,r+g}$, so the DAS cross-correlation for parallel channels that line-up is:

$$\begin{aligned} C_{DAS:s,r} = C_{tt:s,r} - s_X^2(C_{tt:s+g,r} + C_{tt:s,r+g}) \\ -s_X c_X(C_{tr:s+g,r} + C_{rt:s+g,r} - C_{tr:s,r+g} - C_{rt:s,r+g}) \; -c_X^2(C_{rr:s+g,r} + C_{rr:s,r+g}) + C_{tt:s+g,r+g}. \end{aligned}$$

The cross-angle $\theta_{s,r+g} = \pi - \theta_{s+g,r}$ depends on the distance between the two fibers, so that $\theta_{s,r+g}$ goes to $\pi/2$ as the distance between the fibers grows or g shrinks. Thus, as $\theta_{s,r+g} \to \pi/2$, this simplifies to:

$$C_{DAS:s,r} \approx C_{tt:s,r} - C_{tt:s+g,r} - C_{tt:s,r+g} + C_{tt:s+g,r+g},$$

meaning that if the parallel fibers are at least a few gauge lengths apart, we expect to extract a Love wave with a wavelet that is a bit more ringy than the typical $C_{tt:s,r}$.

RESULTS

We tested cross-correlations between lines on SDASA-1. These are data recorded on an OptaSense ODH-3 interrogator unit at a 50 Hz sample rate, 8.16 m channel spacing, and 7.14 m gauge length. As seen in Martin et al. (2017c) and Martin et al. (2017b), we previously tested cross-coherence and cross-correlation as methods to extract Rayleigh waves from channels along the same straight line fiber. To start looking

at response estimates between lines, we initally tried cross-correlation, but found it to not focus energy well enough. We next tested one-bit correlation. The data were first split into 300 second windows with 50% overlap, meaning a new windows starts every 150 seconds, then bandpassed from 0.2 to 24 Hz, then the median of each time sample was subtracted to remove laser noise before the data were thresholded to ± 1.

The correlations for a virtual source at channel 35 can be seen in Figures 2a, 2b, and 2c. The greatest improvement can be seen in the response of channels 50 to 100, a segment perpendicular to 35 (so it should have a mix of Love and Rayleigh waves). In particular, there appear to be two distinct wave speeds along this segment. There's also a strong response on channels 160 to 180, a segment parallel to 35 which shows a much higher velocity event starting around 0.7 seconds lag. Further investigation is needed to determine whether this is truly an extracted Love wave, or something else, perhaps even an event with a higher apparent velocity due to 1D structure of that line.

The correlations for a virtual source at channel 75 can be seen in Figures 3a, 3b, and 3c. This channel is near the crossing point of Via Ortega and Via Pueblo, so in the 72 hour correlation, a slight V can be seen near channel 180 or 190, which is close to channel 75 but oriented in the orthogonal direction. More interestingly, after three days of correlations, two events can be seen running along Via Ortega emanating from channel 75. A slow one that is stronger ata few hundred meters per second, and a fast one (particularly to the south of 75) closer to around one thousand meters per second. Further cross-correlations need to be done to get more certain picks on these velocities.

FUTURE WORK

Further work needs to be done to quantify the convergence rates of the cross-correlations shown, and to analyze longer periods of time. It would be ideal to build further more scalable code into the framework already developed for pSIN (Chen et al., 2016), but so far, we have been unable to obtain the source code of pSIN. Although the cross-correlations worked well in many parts of the array, some areas, particularly near roads or along the big utility tunnel on Lomita Mall did not have very well-focused energy. To help with pre-processing decisions that may effect convergence rates and potential artifact removal, we are working on automatic-noise-detection/classification (Huot et al., 2017). It would also be interesting to see how site-specific these results are by testing these methods on the grid of fibers installed in Fairbanks, AK by LBL and the Corps of Engineers. After we understand the theory for straight fibers better (particularly the role of C_{RT} and C_{TR}, a separate theory could be built off of this for helically wound cables. This kind of theory may also be useful if one or two components of a geophone go out in a very sparse array where wavefield interpolation isn't possible.

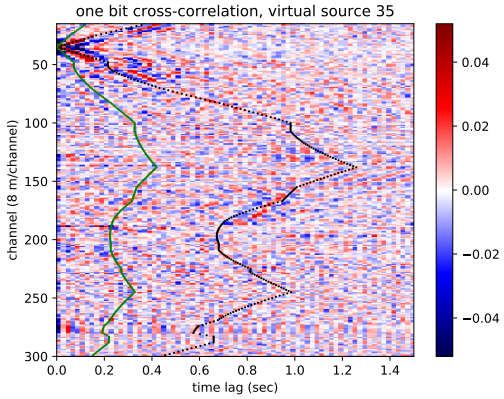

(a)

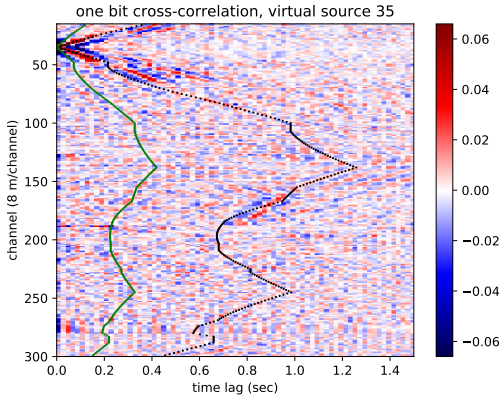

(b)

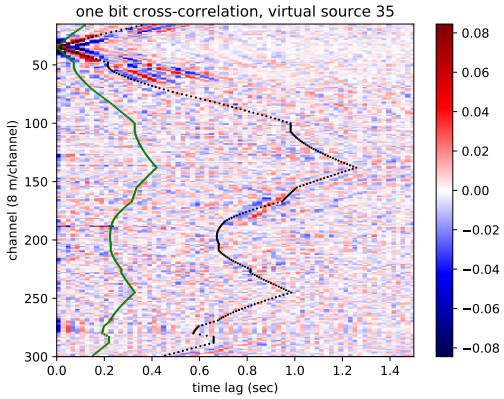

(c)

Figure 2: One-bit correlations of the array against a virtual source at channel 35 on the west-going line in the southwest corner of the array improve from (left) 24 hours of correlations to (right) 72 hours of correlations, and (bottom) to 120 hours. The arrival times of 1200 m/s and 400 m/s waves are overlaid. [**CR**]

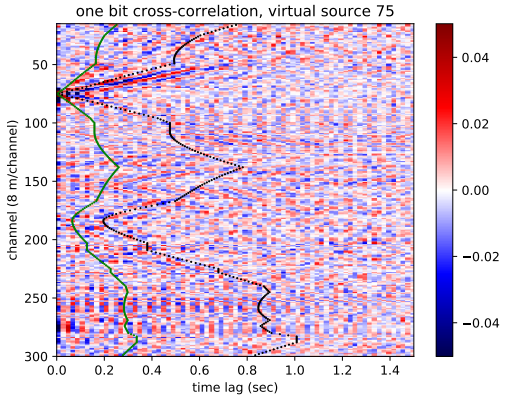

(a)

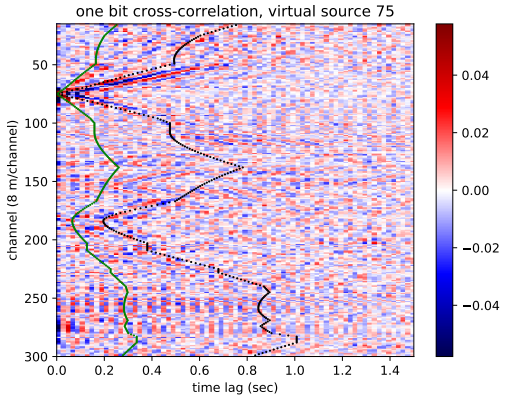

(b)

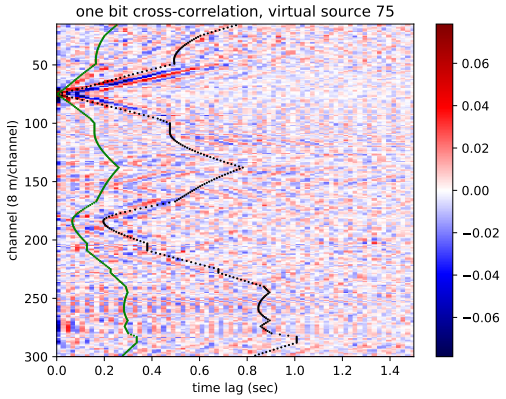

(c)

Figure 3: One-bit correlations of the array against a virtual source at channel 75 in the middle north-going line along Via Ortega. It improves from (left) 24 hours of correlations to (right) 72 hours of correlations, and (bottom) 120 hours. The arrival times of 1200 m/s and 400 m/s waves are overlaid. [**CR**]

CONCLUSIONS

We have extended the theory of ambient noise interferometry to understand cross-correlations of all channels throughout two-dimensional DAS arrays. We have tested this theory on cross-correlations throughout SDASA-1, where we observed several features predicted by our theoretical model. Two particular predicted features observed were a mix of two wave components in cross-correlations between orthogonal lines, and a wave showing up at a reasonable time for a Love wave on a line parallel to the virtual source. Further investigation and verification of this theory should be done so that we can understand how to image with the many additional ray-paths provided by correlations throughout the whole array.

ACKNOWLEDGEMENTS

We thank OptaSense, Inc. for supplying the interrogator unit, and Martin Karrenbach and Steve Cole for their assistance in the installation and guidance in using the data. We thank affiliates of the Stanford Exploration Project for their support. Eileen Martin has also been supported in part by the U.S. DOE under grant No. DE-FG02-97ER25308 and a Schlumberger Innovation Fellowship. We thank our colleagues at Stanford for helpful discussions, particularly Jason Chang, Bob Clapp, Stew Levin and George Papanicolaou. We thank Stanford IT and SEEES IT for assistance running the array, and Stanford Center for Computational Earth and Environmental Sciences for computing resources. This work has been influenced by our collaborations with Lawrence Berkeley National Laboratory where E. Martin is an affiliate, and we have particularly benefited from discussions on DAS interferometry with Jonathan Ajo-Franklin, Nate Lindsey, and Shan Dou.

REFERENCES

Ajo-Franklin, J., N. Lindsey, S. Dou, T. Daley, B. Freifeld, E. Martin, M. Robertson, C. Ulrich, and A. Wagner, 2015, A field test of distributed acoustic sensing for ambient noise recording: Expanded Abstracts of the 85th Ann. Internat. Mtg.

Chen, P., N. Taylor, K. Dueker, I. Keifer, A. Wilson, C. McGuffy, C. Novitsky, A. Spears, and W. Holbrook, 2016, psin: a scalable, parallel algorithm for seismic interferometry of large-n ambient noise data: Computers and Geosciences, **93**.

de Ridder, S., 2014, Passive seismic surface-wave interferometry for reservoir-scale imaging: PhD thesis, Stanford University.

Huot, F., Y. Ma, R. Cieplicki, E. Martin, and B. Biondi, 2017, Automatic noise exploration in urban areas : SEP-Report, **168**, 277–288.

Kuvshinov, B., 2016, Interaction of helically wound fibre-optic cables with plane seismic waves: Geophysical Prospecting, **64**, 671–688.

Lin, F., M. Moschetti, and M. Ritzwoller, 2008, Surface wave tomography of the

western united states from ambient seismic noise: Rayleigh and love wave phase velocity maps: Geophysical Journal International.

Martin, E., J. Ajo-Franklin, S. Dou, N. Lindsey, T. Daley, B. Freifeld, M. Robertson, A. Wagner, and C. Ulrich, 2015, Interferometry of ambient noise from a trenched distributed acoustic sensing array: Expanded Abstracts of the 85th Ann. Internat. Mtg.

Martin, E., B. Biondi, S. Cole, and M. Karrenbach, 2017a, Overview of the Stanford DAS Array-1 (SDASA-1) : SEP-Report, **168**, 1–10.

Martin, E., B. Biondi, M. Karrenbach, and S. Cole, 2017b, Ambient noise interferometry from das array in underground telecommunications conduits: Technical Programme of the 79th Conference & Exhibition.

———, 2017c, Continuous subsurface monitoring by passive seismic with distributed acoustic sensors- the "stanford array" experiment: Proceedings of the First EAGE Workshop on Practical Reservoir Monitoring.

Martin, E., N. Lindsey, S. Dou, J. Ajo-Franklin, A. Wagner, K. Bjella, T. Daley, B. Freifeld, M. Robertson, and C. Ulrich, 2016, Interferometry of a roadside das array in fairbanks, ak: Expanded Abstracts of the 86th Ann. Internat. Mtg.

Nakata, N., J. Chang, J. Lawrence, and P. Boué, 2015, Body wave extraction and tomography at long beach, california, with ambient-noise interferometry: J. Geophys. Res. Solid Earth, **120**, 1159–1173.

Nakata, N., R. Snieder, T. Tsuji, K. Larner, and T. Matsuoka, 2011, Shear wave imaging from traffic noise using seismic interferometry by cross-coherence: Geophysics, **76**, SA97–SA106.

Shapiro, N., M. Campillo, L. Stehly, and M. Ritzwoller, 2005, High-resolution surface-wave tomography from ambient seismic noise: Science, **307**, 1615–1618.

Zeng, X., C. Thurber, H. Wang, D. Fratta, E. Matzel, and P. Team, 2017, High-resolution shallow structure revealed with ambient noise tomography on a dense array: Proceedings, 42nd Workshop on Geothermal Reservoir Engineering.